Applied Thermal Engineering 72 (2014) 56–61

Contents lists available at ScienceDirect

Applied Thermal Engineering

journal homepage: www.elsevier.com/locate/apthermeng

Thermodynamic consistency of the pseudopotential lattice Boltzmann model for simulating liquid–vapor flows

Q. Li [a], K.H. Luo [b,*]

[a] Energy Technology Research Group, Faculty of Engineering and the Environment, University of Southampton, Southampton SO17 1BJ, United Kingdom
[b] Department of Mechanical Engineering, University College London, University of London, Torrington Place, London WC1E 7JE, United Kingdom

HIGHLIGHTS

- The effect of the Laplace's law on the thermodynamic consistency is investigated.
- The dependence of ρ_V on the droplet size can be reduced when θ_V increases.
- The interface thickness is related to the slope of the mechanically unstable region.

ARTICLE INFO

Article history:
Received 30 September 2013
Accepted 16 March 2014
Available online 31 March 2014

Keywords:
Lattice Boltzmann method
Pseudopotential model
Liquid–vapor flow
Thermodynamic consistency

ABSTRACT

In this paper, the effects of the equation of state on the thermodynamic consistency and the interface thickness are examined in the pseudopotential lattice Boltzmann modeling of liquid–vapor flows. It is shown that, with the increase of the slope of the equation of state in the vapor-phase region (θ_V), the influence of the droplet size on the vapor density can be reduced. Numerically, it is found that, when the vapor-phase sound speed ($\sqrt{\theta_V}$) is of the same order of magnitude as the lattice sound speed (c_s), the vapor density can be generally kept around its equilibrium value. Hence, to achieve thermodynamically consistent simulations, the vapor-phase sound speed should be comparable with the lattice sound speed. Furthermore, the interface thickness in the pseudopotential LB modeling is found to be related to the slope of the equation of state in the mechanically unstable region (θ_M). It is shown that $|\theta_M|$ should be decreased when the interface thickness needs to be widened to reduce the spurious currents.

1. Introduction

In the past two decades, the lattice Boltzmann (LB) method, which is based on the mesoscopic kinetic equation for particle distribution functions, has been developed into an alternative approach for simulating fluid flows [1–6] and solving partial differential equations [7,8]. Owing to its kinetic nature, the LB method has been found to be pretty useful for modeling multiphase flows, which is an important subject of fundamental and applied scientific research with applications to a wide variety of industrial and natural processes [1,4,9,10].

The existing multiphase LB models can be generally classified into four categories: the color-gradient model [11,12], the pseudopotential model [13,14], the free-energy model [15–17], and the kinetic-theory-based model [18,19]. Among these models, the pseudopotential multiphase model proposed by Shan and Chen [13,14] is a very popular model in the LB community. In this model, the fluid interactions are mimicked by an interparticle potential and the phase separation is achieved via a short-range attraction between different phases. As a consequence, in the pseudopotential LB modeling of multiphase flows the phase segregation can emerge naturally without tracking or capturing the interfaces between different phases, which is often required in traditional numerical approaches. Although the pseudopotential LB model has attracted much attention because of its simplicity and computational efficiency, it has also received considerable criticism on the lack of thermodynamic consistency and the large spurious currents [20].

It is well-known that, in the pseudopotential LB model, the coexistence densities (the liquid and vapor densities) are related to the mechanical stability condition of the model. However, in the thermodynamic theory the coexistence densities are determined by the Maxwell construction. Generally, the coexistence densities given by the mechanical stability condition of the pseudopotential LB model are inconsistent with the solution obtained with the

* Corresponding author.
E-mail address: K.Luo@ucl.ac.uk (K.H. Luo).

http://dx.doi.org/10.1016/j.applthermaleng.2014.03.030

Maxwell construction. Recently, we found [21,22] that in the pseudopotential LB model the thermodynamic consistency can be approximately achieved by adjusting the mechanical stability condition. Nevertheless, for circular/spherical interfaces, the droplet or bubble size will also affect the thermodynamic consistency of the system through the Laplace's law [9]. As a result, the coexistence densities (especially the vapor density) often vary with the droplet/bubble size significantly.

In the present study, the influences of the equation of state in the pseudopotential LB modeling of liquid–vapor flows are examined. To be specific, we will investigate the effects of the equation of state on the thermodynamic consistency and the interface thickness. We will show how to adjust the equation of state to reduce the dependence of the coexistence densities on the droplet size and how to widen the interface thickness to minimize the spurious currents. The rest of the present paper is organized as follows. Firstly, the pseudopotential LB model with an improved forcing scheme is introduced in Section 2. Numerical results will be given in Section 3. A brief conclusion is finally made in Section 4.

2. The pseudopotential LB model

The two-dimensional nine-velocity (D2Q9) LB model with a multiple-relaxation-time (MRT) collision operator [23] is considered. The MRT LB equation is given by

$$f_\alpha(\mathbf{x}+\mathbf{e}_\alpha\delta_t, t+\delta_t) = f_\alpha(\mathbf{x},t) - \left(\mathbf{M}^{-1}\mathbf{\Lambda}\mathbf{M}\right)_{\alpha\beta}\left(f_\beta - f_\beta^{eq}\right) + \delta_t F'_\alpha. \tag{1}$$

where $\mathbf{\Lambda} = \mathrm{diag}(\tau_\rho^{-1}, \tau_e^{-1}, \tau_\varsigma^{-1}, \tau_j^{-1}, \tau_q^{-1}, \tau_j^{-1}, \tau_q^{-1}, \tau_\nu^{-1}, \tau_\nu^{-1})$ is the diagonal Matrix, $\mathbf{M}$ is the orthogonal transformation matrix, and F'_α represents the forcing term in the velocity space. Using the transformation matrix, the right hand side of Eq. (1) can be rewritten as [24]

$$\mathbf{m}^* = \mathbf{m} - \mathbf{\Lambda}(\mathbf{m}-\mathbf{m}^{eq}) + \delta_t\left(\mathbf{I} - \frac{\mathbf{\Lambda}}{2}\right)\mathbf{S}, \tag{2}$$

where $\mathbf{I}$ is the unit tensor, $\mathbf{S}$ is the forcing term in the moment space with $(\mathbf{I}-0.5\mathbf{\Lambda})\mathbf{S} = \mathbf{M}\mathbf{F}\prime$, and the equilibria $\mathbf{m}^{eq}$ is given by

$$\mathbf{m}^{eq} = \rho\left(1, -2+3|\mathbf{v}|^2, 1-3|\mathbf{v}|^2, v_x, -v_x, v_y, -v_y, v_x^2-v_y^2, v_xv_y\right)^{\mathrm{T}}. \tag{3}$$

The streaming process of the MRT LB equation is given by

$$f_\alpha(\mathbf{x}+\mathbf{e}_\alpha\delta_t, t+\delta_t) = f_\alpha^*(\mathbf{x},t), \tag{4}$$

where $\mathbf{f}^* = \mathbf{M}^{-1}\mathbf{m}^*$. The macroscopic density and velocity are calculated via

$$\rho = \sum_\alpha f_\alpha, \quad \rho\mathbf{v} = \sum_\alpha \mathbf{e}_\alpha f_\alpha + \frac{\delta_t}{2}\mathbf{F}. \tag{5}$$

Here $\mathbf{F} = (F_x, F_y)$ is the interaction force [25]

$$\mathbf{F} = -G\psi(\mathbf{x})\sum_{\alpha=1}^{8} w\left(|\mathbf{e}_\alpha|^2\right)\psi(\mathbf{x}+\mathbf{e}_\alpha)\mathbf{e}_\alpha, \tag{6}$$

where ψ is the pseudopotential, G is the interaction strength, and $w(|\mathbf{e}_\alpha|^2)$ are the weights, which are given by $w(1) = 1/3$ and $w(2) = 1/12$ for the nearest-neighbor interactions on the D2Q9 lattice.

In Shan-Chen's original pseudopotential LB model, the pseudopotential ψ is defined as $\psi = \psi_0\exp(-\rho_0/\rho)$, which is usually limited to low-density-ratio multiphase flows. To achieve high density ratios, the pseudopotential can be chosen as $\psi = \sqrt{2(p(\rho)-\rho c_s^2)/Gc^2}$ [21,26], where $c_s = c/\sqrt{3}$ is the lattice sound speed and $p(\rho)$ represents a desired equation of state, such as the Carnahan-Starling equation of state. Nevertheless, with such a choice, the pseudopotential LB model will suffer from the lack of thermodynamic consistency because the coexistence densities given by the model are inconsistent with the solution given by the Maxwell construction. Recently, we found that in this case the thermodynamic consistency can be approximately achieved by adjusting the mechanical stability condition [21,22], which can be implemented via an improved forcing scheme. For the MRT pseudopotential LB model, the improved forcing scheme is given as follows [22]:

$$\mathbf{S} = \begin{bmatrix} 0 \\ 6(v_xF_x+v_yF_y) + \dfrac{12\sigma|\mathbf{F}|^2}{\psi^2\delta_t(\tau_e-0.5)} \\ -6(v_xF_x+v_yF_y) - \dfrac{12\sigma|\mathbf{F}|^2}{\psi^2\delta_t(\tau_\varsigma-0.5)} \\ F_x \\ -F_x \\ F_y \\ -F_y \\ 2(v_xF_x-v_yF_y) \\ (v_xF_y+v_yF_x) \end{bmatrix}, \tag{7}$$

where $|\mathbf{F}|^2 = (F_x^2+F_y^2)$ and σ is used to tune the mechanical stability condition.

3. Numerical results and discussion

3.1. Equation of state

In the present study, a piecewise linear equation of state [27] is adopted for non-ideal fluids:

$$p(\rho) = \begin{cases} \rho\theta_V & \text{if } \rho \le \rho_1 \\ \rho_1\theta_V + (\rho-\rho_1)\theta_M & \text{if } \rho_1 < \rho \le \rho_2, \\ \rho_1\theta_V + (\rho_2-\rho_1)\theta_M + (\rho-\rho_2)\theta_L & \text{if } \rho > \rho_2 \end{cases} \tag{8}$$

where $\theta_V = (\partial p/\partial\rho)_V$, $\theta_L = (\partial p/\partial\rho)_L$, and $\theta_M = (\partial p/\partial\rho)_M$ are the slopes of $p(\rho)$ in the vapor-phase region, the liquid-phase region, and the mechanically unstable region, respectively ($\theta_V > 0$ and $\theta_L > 0$, while $\theta_M < 0$). Meanwhile, $\sqrt{\theta_V}$ and $\sqrt{\theta_L}$ represent the sound speeds of the vapor-phase and the liquid-phase, respectively. The unknown variables ρ_1 and ρ_2, which define the spinodal points, are obtained by solving two equations [27]: one for determining mechanical equilibrium

$$\int_{\rho_V^e}^{\rho_L^e} \mathrm{d}p(\rho) = p(\rho_L^e) - p(\rho_V^e) = (\rho_1-\rho_V^e)\theta_V + (\rho_2-\rho_1)\theta_M + (\rho_L^e-\rho_2)\theta_L = 0, \tag{9}$$

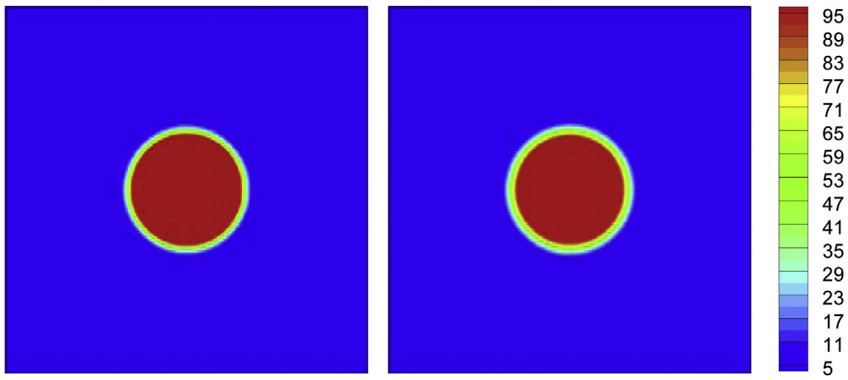

Fig. 1. Density contours of Case O (left) and Case A (right) at $R = 20$.

and the other for chemical equilibrium

$$\int_{\rho_V^e}^{\rho_L^e} \frac{1}{\rho} \mathrm{d}p(\rho) = \log(\rho_1/\rho_V^e)\theta_V + \log(\rho_2/\rho_1)\theta_M + \log(\rho_L^e/\rho_2)\theta_L = 0, \tag{10}$$

where ρ_V^e and ρ_L^e are the vapor density and liquid density, respectively. Note that, in the derivation of Eq. (10), the Maxwell construction has been used

$$\int_{\rho_V^e}^{\rho_L^e} \frac{1}{\rho^2}[p(\rho) - p(\rho_V^e)]\mathrm{d}\rho = \int_{\rho_V}^{\rho_L} [p(\rho) - p(\rho_V^e)]\mathrm{d}\left(-\frac{1}{\rho}\right) = \int_{\rho_V^e}^{\rho_L^e} \frac{1}{\rho}\mathrm{d}p(\rho) = 0. \tag{11}$$

In Ref. [27], the parameters θ_V, θ_L, and θ_M are given as follows (Case O):

$$\theta_V = 0.04c_s^2, \quad \theta_L = c_s^2, \quad \theta_M = -0.36c_s^2. \tag{12}$$

When ρ_V^e and ρ_L^e are given, the unknown variables ρ_1 and ρ_2 can be determined by Eqs. (9), (10) and (12). For example, when $\rho_V^e = 1$ and $\rho_L^e = 100$, Eq. (12) leads to $\rho_1 = 34.29$ and $\rho_2 = 83.59$.

3.2. Numerical analyses via the simulation of circular droplets

Now we investigate the influences of the equation of state in the pseudopotential LB modeling of liquid–vapor flows. Specifically, we will show the effects of the parameters θ_V and θ_M in Eq. (8) on the thermodynamic consistency and the interface thickness, respectively. The liquid-phase sound speed is fixed at $\sqrt{\theta_L} = c_s$. The problem of stationary circular droplets is simulated. A $N_x \times N_y = 120 \times 120$ lattice system is employed and a circular droplet with a radius of R is initially placed at the center of the domain with the liquid phase inside the droplet. The periodical boundary conditions are applied in the x- and y-directions. The pseudopotential $\psi(\rho)$ is given by $\psi = \sqrt{2(p(\rho) - \rho c_s^2)/Gc^2}$. The requirement for G is to ensure that the whole term inside the square root is positive [9]. In the present study, G is set to -1. The relaxation times are chosen as : $\tau_\rho = \tau_j = 1.0$, $\tau_e^{-1} = \tau_\varsigma^{-1} = 1.1$, and $\tau_q^{-1} = 1.1$.

To display the effect of the parameter θ_M, the following case is considered:

$$\text{Case A}: \quad \theta_V = 0.04c_s^2, \quad \theta_L = c_s^2, \quad \theta_M = -0.06c_s^2. \tag{13}$$

The original case given by Eq. (12) is referred as Case O. According to Eq. (9) and Eq. (10), the variables ρ_1 and ρ_2 in Eq. (8) are given by $\rho_1 = 9.4$ and $\rho_2 = 95.19$ for Case A. The density contours of Cases O and A with $R = 20$ and $R = 40$ are shown in Figs. 1 and 2, respectively. From the figures it can be seen that the interface thickness of Case A is larger than that of Case O. To show this point more clearly, local details of the density contours of Cases O and A at $R = 40$ are illustrated in Fig. 3, from which we can find that the

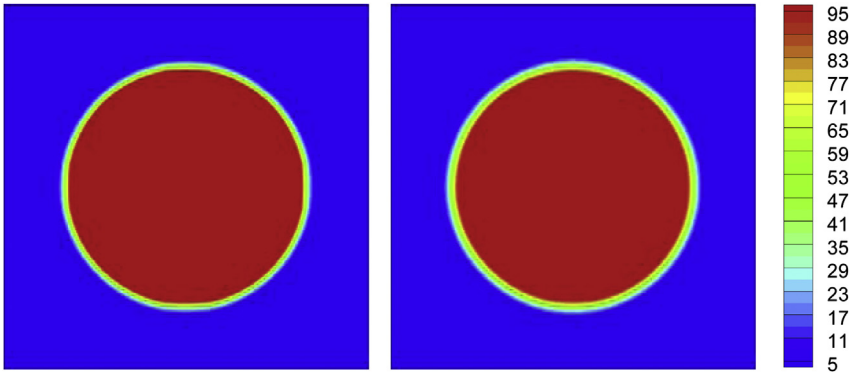

Fig. 2. Density contours of Case O (left) and Case A (right) at $R = 40$.

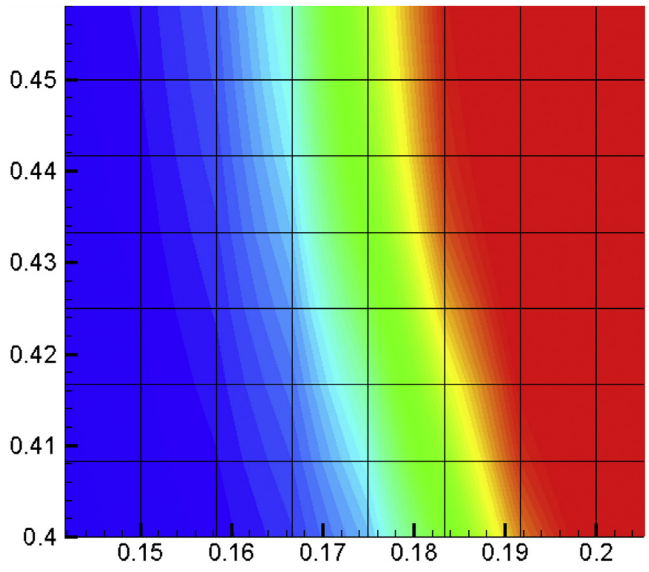

(a) Case O

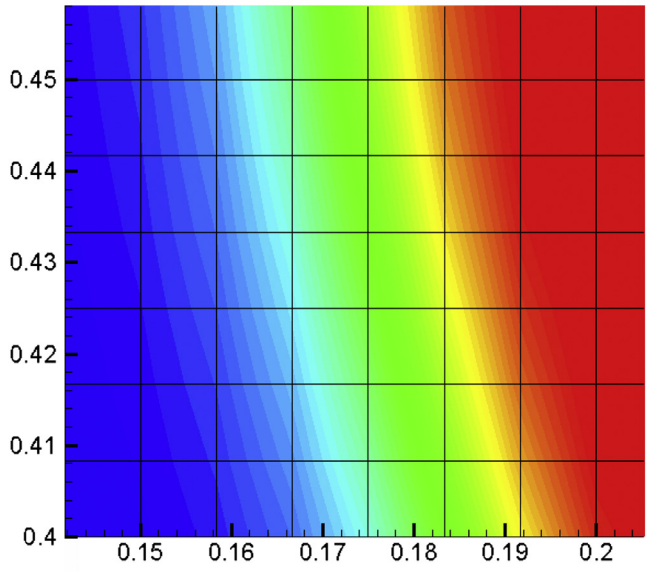

(b) Case A

Fig. 3. Local details of the density contours of Case O and Case A at $R = 40$.

interface thicknesses of Cases O and A are around 3.5 l.u and 5 l.u., respectively, where l.u. denotes lattice units. Meanwhile, it is found that, from Case O to Case A, the maximum magnitude of the spurious currents is significantly reduced from 0.032 to 0.002 with the increase of the interface thickness. Actually, in the literature, some previous studies of multiphase LB models have shown that [28,29] the interface thickness in the LB modeling of multiphase flows should be around 4–5 lattices in order to achieve a reliable solution. According to the numerical results as well as Eqs. (12) and (13), we can conclude that the interface thickness in the pseudopotential LB model can be enlarged by decreasing $|\theta_M|$.

On the basis of Case A, another case can be considered to investigate the effect of θ_V:

$$\text{Case B}: \quad \theta_V = 0.49c_s^2, \quad \theta_L = c_s^2, \quad \theta_M = -0.06c_s^2. \tag{14}$$

By comparing Eq. (14) with Eq. (13), we can see that the vapor-phase sound speed has been increased from $\sqrt{\theta_V} = 0.2c_s$ to $0.7c_s$. When $\rho_V^e = 1$ and $\rho_L^e = 100$, Case B corresponds to $\rho_1 = 1.49$ and $\rho_2 = 94.65$. Three different radii are studied: $R = 40$, $R = 25$, and $R = 12.5$. The test of $R = 40$ is taken as the standard test. In other words, the parameter σ in Eq. (7) is adjusted to achieve thermodynamic consistency ($\rho_V \approx 1$ and $\rho_L \approx 100$) in the test of $R = 40$. Hence σ in Eq. (7) is set to 0.1116 and 0.087 for Cases A and B, respectively. The coexistence densities of the two cases are listed in Table 1. From the table we can see that the liquid densities agree well with the prescribed liquid density $\rho_L^e = 100$ for both Case A and Case B. However, the vapor densities of Case A significantly vary with the droplet size, while the results of Case B are basically in good agreement with the prescribed vapor density $\rho_V^e = 1$. Specifically, at $R = 12.5$ the relative errors (vapor-phase) of Cases A and B are about 61% and 6%, respectively.

From Eqs. (13) and (14), it can be seen that the main difference between Case A and Case B lies in that the vapor-phase sound speed of Case B is of the same order of magnitude as the lattice sound speed (c_s), whereas the vapor-phase sound speed of Case A is much smaller than c_s. For flat interfaces, the thermodynamic consistency of the pseudopotential LB model is completely determined by the mechanical stability condition. However, for circular interfaces, the Laplace's law [9]

$$p_L - p_V = \frac{\vartheta}{R} \tag{15}$$

will also affect the thermodynamic consistency of the system.

In Eq. (15), ϑ is the surface tension; p_L and p_V are the pressures of the liquid and vapor phases, respectively, which can be described as follows [9]:

$$p_L = p_L^e + \frac{\rho_L^e}{\rho_L^e - \rho_V^e}\left(\frac{\vartheta}{R}\right), \quad p_V = p_V^e + \frac{\rho_V^e}{\rho_L^e - \rho_V^e}\left(\frac{\vartheta}{R}\right) \tag{16}$$

The superscript e denotes the prescribed properties given by the Maxwell construction. For simplicity, we assume that the pressure difference $\Delta p_V = (p_V - p_V^e)$ can be defined as $\Delta p_V = (\rho_V - \rho_V^e)\left(\sqrt{(\partial p/\partial\rho)_V}\right)^2$, in which $\sqrt{(\partial p/\partial\rho)_V} = \sqrt{\theta_V}$ is the sound speed in the vapor-phase region. Then we can obtain

$$\rho_V - \rho_V^e = \frac{1}{\theta_V}\frac{\rho_V^e}{\rho_L^e - \rho_V^e}\left(\frac{\vartheta}{R}\right) \tag{17}$$

Obviously, when ϑ and θ_V are given, the density deviation $\Delta\rho_V = (\rho_V - \rho_V^e)$ will increase with the decrease of R. Meanwhile, it can be seen that a larger θ_V will lead to a smaller difference between ρ_V and ρ_V^e. This is the reason why from Case A to Case B the deviation of the vapor density can be lowered from 61% to 6%: θ_V has been increased from $\theta_V = 0.04c_s^2$ to $0.49c_s^2$. To sum up, we have shown that, in the pseudopotential LB modeling of liquid–vapor flows, the sound speed of the vapor phase should be comparable with lattice sound speed so as to reduce the dependence of the vapor density on the droplet size.

Table 1
The coexistence densities of Cases A and B at $R = 40$, 25, and 12.5.

R	ρ_V		ρ_L	
	Case A	Case B	Case A	Case B
40	1.001	1.004	100.11	100.14
25	1.151	1.019	100.17	100.21
12.5	1.609	1.060	100.35	100.42

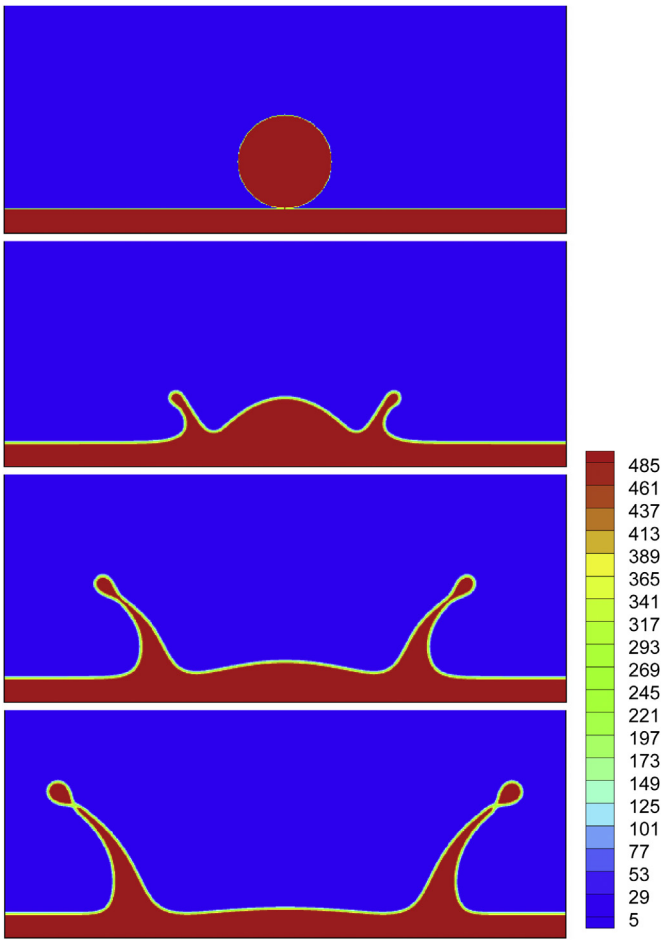

Fig. 4. The impingement process of droplet splashing on a thin liquid film at $\rho_L^e/\rho_V^e = 500$ and $Re = 500$. From top to bottom: $t = 0$, $500\delta_t$, $1100\delta_t$, and $1600\delta_t$.

3.3. Droplet splashing

In this subsection, a dynamic problem is considered to show the dynamic variations of the densities: droplet splashing on a thin liquid film. The splashing of droplets on liquid/solid surfaces is a crucial event in a wide variety of phenomena, such as the raindrop splashing on the ground, the impact of a fuel droplet on the wall of a combustion chamber, and nano-printing using the laser induced forward transfer technique [22,28].

The lattice system is chosen as $N_x \times N_y = 600 \times 250$. The liquid film is placed at the bottom of the computational domain and its height is one-tenths of the entire domain height. The radius of the droplet is $R = 50$ and its impact velocity is $(v_x,v_y) = (0,-U)$, where $U = 0.125$ ($\delta_t = 1$). The no-slip boundary condition is imposed at the bottom wall, while the open boundary condition is applied at other boundaries. To show the capability of the model for simulating large-density-ratio multiphase flows, the liquid and vapor densities are taken as $\rho_L^e = 500$ and $\rho_V^e = 1$, respectively.

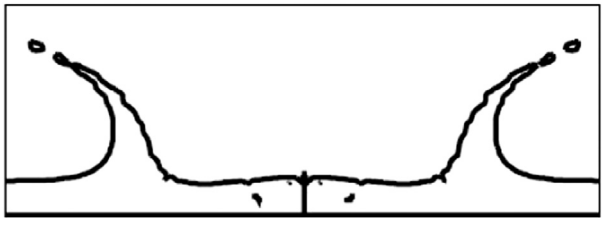

Fig. 5. Local detail of droplet splashing on a thin liquid film shown in Ref. [30].

Table 2
The minimum and maximum densities during the impingement process of droplet splashing.

t	$200\delta_t$	$400\delta_t$	$800\delta_t$	$1200\delta_t$	$1600\delta_t$
ρ_{min}	0.945	0.906	0.914	0.928	0.933
ρ_{max}	538.9	507.6	511.9	506.3	521.0

Following the analyses in the above section, the parameters θ_V, θ_L, and θ_M are chosen as follows:

$$\theta_V = 0.64c_s^2, \quad \theta_L = c_s^2, \quad \theta_M = -0.04c_s^2. \tag{18}$$

According to Eqs. (9) and (10), ρ_1 and ρ_2 are given by $\rho_1 = 1.36$ and $\rho_2 = 481.04$. The parameter σ in Eq. (7) is taken as 0.084. The Reynolds number $Re = UD/\upsilon_L$ is set to 500 with $\upsilon_L = 0.025$. The kinematic viscosity ratio between the vapor and liquid phases is fixed at $\upsilon_V/\upsilon_L = 20$. For simplicity, the viscosity in the simulations is chosen as $\upsilon(\rho) = \upsilon_L$ for $\rho > (\rho_L^e + \rho_V^e)/2$ and $\upsilon(\rho) = \upsilon_V$ for $\rho \le (\rho_L^e + \rho_V^e)/2$.

The snapshots of the impingement process are shown in Fig. 4, from which it can be seen that, after the impact, a thin liquid sheet will be formed in the region located at the intersection between the droplet and the liquid layer. Later, the sheet evolves into a lamella whose end-rim is unstable and will break-up into secondary droplets, which is an important phenomenon of droplet splashing and can be seen in Fig. 3 at $t = 1600\delta_t$. The observed main features are in good agreement with the solution obtained by the volume-of-fluid method in Ref. [30], which is shown in Fig. 5 for comparison. The minimum density ρ_{min} and the maximum density ρ_{max} at $t = 400\delta_t$, $200\delta_t$, $800\delta_t$, $1200\delta_t$, and $1600\delta_t$ are listed in Table 2. As can be seen, the variations of the minimum and maximum densities are basically within 10% of the corresponding prescribed densities ($\rho_V^e = 1$ and $\rho_L^e = 500$).

4. Conclusions

In this paper, we have studied the influences of the equation of state on the thermodynamic consistency and the interface thickness in the pseudopotential LB modeling of liquid–vapor flows. We have shown that the dependence of the vapor density on the droplet size can be reduced with the increase of the slope of the equation of state in the vapor-phase region (θ_V), which can be seen from Eq. (17). Through the numerical simulations of stationary circular droplets, we found that the vapor density can be generally kept around its equilibrium value when $\sqrt{\theta_V}$ is comparable with the lattice sound speed (c_s), e.g., at $R = 12.5$ the deviation of the density is lowered from 61% to 6% when $\sqrt{\theta_V}$ increases from $0.2c_s$ to $0.7c_s$.

Meanwhile, it has been shown that the interface thickness is related to the slope of the equation of state in the mechanically unstable region (θ_M). When $|\theta_M|$ decreases, the interface thickness is found to be widened. Furthermore, to show the dynamic variations of the densities, the problem of droplet splashing on a thin liquid film at $\rho_L^e/\rho_V^e = 500$ has been simulated. The main features of the impingement process of droplet splashing agree well with previous studies. Owing to the use of a vapor-phase sound speed comparable with the lattice sound speed, the deviations of the densities are within 10%.

Acknowledgements

Support by the Engineering and Physical Sciences Research Council of the United Kingdom under Grant Nos. EP/I012605/1 and EP/J016381/2 is gratefully acknowledged.

References

[1] S. Chen, G.D. Doolen, Lattice Boltzmann method for fluid flows, Annu. Rev. Fluid Mech. 30 (1998) 329–364.
[2] R. Benzi, S. Succi, M. Vergassola, The lattice Boltzmann equation: theory and applications, Phys. Rep. 222 (1992) 145–197.
[3] D. Yu, R. Mei, L.-S. Luo, W. Shyy, Viscous flow computations with the method of lattice Boltzmann equation, Prog. Aerosp. Sci. 39 (2003) 329–367.
[4] C.K. Aidun, J.R. Clausen, Lattice-Boltzmann method for complex flows, Annu. Rev. Fluid Mech. 42 (2010) 439–472.
[5] K. Suga, Lattice Boltzmann methods for complex micro-flows: applicability and limitations for practical applications, Fluid Dyn. Res. 45 (2013) 034501.
[6] Y. Wang, Y.L. He, Q. Li, Lattice Boltzmann model for viscous compressible flows with high Mach number, in: First Asian Symposium on Computational Heat Transfer and Fluid Flow, Xi'an, China, Oct. 18–21, 2007.
[7] H. Lai, C. Ma, The lattice Boltzmann model for the second-order Benjamin-Ono equations, J. Stat. Mech. Theory Exp. (2010) P04011.
[8] H. Lai, C. Ma, Lattice Boltzmann model for generalized nonlinear wave equations, Phys. Rev. E 84 (2011) 046708(1)–046708(12).
[9] E.S. Kikkinides, A.G. Yiotis, M.E. Kainourgiakis, A.K. Stubos, Thermodynamic consistency of liquid-gas lattice Boltzmann methods: Interfacial property issues, Phys. Rev. E 78 (2008) 036702(1)–036702(16).
[10] Y.Y. Yan, Y.Q. Zu, B. Dong, LBM, a useful tool for mesoscale modelling of single-phase and multiphase flow, Appl. Therm. Eng. 31 (2011) 649–655.
[11] A.K. Gunstensen, D.H. Rothman, S. Zaleski, G. Zanetti, Lattice Boltzmann model of immiscible fluids, Phys. Rev. A 43 (1991) 4320–4327.
[12] D. Grunau, S. Chen, K. Eggert, A lattice Boltzmann model for multiphase fluid flows, Phys. Fluids A 5 (1993) 2557–2562.
[13] X. Shan, H. Chen, Lattice Boltzmann model for simulating flows with multiple phases and components, Phys. Rev. E 47 (1993) 1815–1819.
[14] X. Shan, H. Chen, Simulation of nonideal gases and liquid-gas phase transitions by the lattice-Boltzmann equation, Phys. Rev. E 49 (1994) 2941–2948.
[15] M.R. Swift, W.R. Osborn, J.M. Yeomans, Lattice Boltzmann simulation of nonideal fluids, Phys. Rev. Lett. 75 (1995) 830–833.
[16] M.R. Swift, E. Orlandini, W.R. Osborn, J.M. Yeomans, Lattice Boltzmann simulations of liquid-gas and binary fluid systems, Phys. Rev. E 54 (1996) 5041–5052.
[17] T. Inamuro, T. Ogata, S. Tajima, N. Konishi, A lattice Boltzmann method for incompressible two-phase flows with large density differences, J. Comput. Phys. 198 (2004) 628–644.
[18] X. He, X. Shan, G.D. Doolen, Discrete Boltzmann equation model for nonideal gases, Phys. Rev. E 57 (1998) R13–R16.
[19] X. He, G.D. Doolen, Thermodynamic foundations of kinetic theory and lattice Boltzmann models for multiphase flows, J. Stat. Phys. 107 (2002) 309–328.
[20] M. Sbragaglia, R. Benzi, L. Biferale, S. Succi, K. Sugiyama, F. Toschi, Generalized lattice Boltzmann method with multirange pseudopotential, Phys. Rev. E 75 (2007) 026702(1)–026702(13).
[21] Q. Li, K.H. Luo, X.J. Li, Forcing scheme in pseudopotential lattice Boltzmann model for multiphase flows, Phys. Rev. E 86 (2012) 016709(1)–016709(9).
[22] Q. Li, K.H. Luo, X.J. Li, Lattice Boltzmann modeling of multiphase flows at large density ratio with an improved pseudopotential model, Phys. Rev. E 87 (2013) 053301(1)–053301(11).
[23] P. Lallemand, L.-S. Luo, Theory of the lattice Boltzmann method: dispersion, dissipation, isotropy, Galilean invariance, and stability, Phys. Rev. E 61 (2000) 6546–6562.
[24] Q. Li, Y.L. He, G.H. Tang, W.Q. Tao, Improved axisymmetric lattice Boltzmann scheme, Phys. Rev. E 81 (2010) 056707(1)–056707(10).
[25] X. Shan, Pressure tensor calculation in a class of nonideal gas lattice Boltzmann models, Phys. Rev. E 77 (2008) 066702(1)–066702(6).
[26] P. Yuan, L. Schaefer, Equations of state in a lattice Boltzmann model, Phys. Fluids 18 (2006) 042101(1)–042101(11).
[27] C.E. Colosqui, G. Falcucci, S. Ubertini, S. Succi, Mesoscopic simulation of non-ideal fluids with self-tuning of the equation of state, Soft Matter 8 (2012) 3798–3809.
[28] T. Lee, C.-L. Lin, A stable discretization of the lattice Boltzmann equation for simulation of incompressible two-phase flows at high density ratio, J. Comput. Phys. 206 (2005) 16–47.
[29] H.W. Zheng, C. Shu, Y.T. Chew, A lattice Boltzmann model for multiphase flows with large density ratio, J. Comput. Phys. 218 (2006) 353–371.
[30] R. Purvis, F.T. Smith, Droplet impact on water layers: post-impact analysis and computations, Philos. Trans. R. Soc. 363 (2005) 1209–1221.